Nanoscale

PAPER

View Article Online
View Journal | View Issue

Cite this: *Nanoscale*, 2022, **14**, 5194

Altering singlet fission pathways in perylene-dimers; perylene-diimide *versus* perylene-monoimide†

Ilias Papadopoulos, [a] David Gutiérrez-Moreno, [b] Yifan Bo,[a,c] Rubén Casillas,[a,c] Phillip M. Greißel, [a] Timothy Clark, [c] Fernando Fernández-Lázaro *[b] and Dirk M. Guldi *[a]

We used a systematic approach to shed light on the inherent differences in perylenes, namely monoimides *versus* diimides, including coplanarity and dipole moment, and their impact on singlet fission (SF) by designing, synthesizing, and probing a full fledged series of phenylene- and naphthalene-linked dimers. Next to changing the functionality of the perylene core, we probed the effect of the spacers and their varying degrees of rotational freedom, molecular electrostatic potentials, and intramolecular interactions on the SF-mechanism and -efficiencies. An arsenal of spectroscopic techniques revealed that for perylene-monoimides, a strong charge-transfer mixing with the singlet and triplet excited states restricts SF and yields low triplet quantum yields. This is accompanied by an up-conversion channel that includes geminate triplet–triplet recombination. Using perylene-diimides alters the SF-mechanism by populating a charge-separated-state intermediate, which either favors or shuts-down SF. Napthylene-spacers bring about higher triplet quantum yields and overall better SF-performance for all perylene-monoimides and perylene-diimides. The key to better SF-performance is rotational freedom because it facilitates the overall excited-state polarization and amplifies intramolecular interactions between chromophores.

Received 30th December 2021,
Accepted 11th March 2022

DOI: 10.1039/d1nr08523a

rsc.li/nanoscale

Introduction

New and innovative strategies are necessary to overcome the so-called photoelectric limit, a theoretical threshold that describes limitations in power-conversion efficiency in single p–n junction solar cells.[1,2] One such strategy uses singlet fission (SF). In SF, a singlet excited state (S_1) is down-converted into two lower-energy and separated triplet excited states (T_1 + T_1).[3–7] Such a singlet-to-triplet transition starts at (S_1S_0) and proceeds *via* a correlated triplet pair $^1(T_1T_1)$, in which the spin multiplicity is maintained. This renders the generation of $^1(T_1T_1)$ rapid and efficient, in contrast to conventional intersystem crossing (ISC).[8–11]

For SF to occur, the molecular system must meet a number of criteria. These include, among others, matching the energies of (S_1) and (T_1) so that $E(S_1) \geq 2E(T_1)$. Its difference determines the thermodynamic driving force of SF.[8–11] Electronic communication is ensured either by crystal packing in the solid state or high concentration in solution and governs intermolecular SF.[12–19] A drastically different approach involves the use of molecular dimers, for which SF is intramolecular (i-SF) and the molecular spacers influence the SF mechanism, its rates, efficiencies, and quantum yields.[18,20–25]

Mechanistically, SF proceeds mainly *via* two general pathways: one in which the initial (S_1S_0) state transforms directly into $^1(T_1T_1)$, or the second, in which an intermediate state is populated prior to $^1(T_1T_1)$. In most cases, this intermediate state might be a charge transfer (CT) state, either virtual or real, or even a charge separated (CS) state.[13,23,26–32] Once formed, $^1(T_1T_1)$ is subject to spin decoherence, which sets up the path to two separated triplet excited states (T_1 + T_1). If the electronic coupling is, however, too strong, spin decoherence is no longer inactive. Instead, either triplet–triplet annihilation (TTA), by which the electronic ground state is recovered, takes over, or up-conversion *via* geminate triplet–triplet recombination (G-TTA-UC) occurs to yield (S_1S_0).[33,34,35–42,43]

[a]*Department of Chemistry and Pharmacy & Interdisciplinary Center for Molecular Materials (ICMM), Friedrich-Alexander-University Erlangen-Nuremberg, Egerlandstraße 3, 91058 Erlangen, Germany. E-mail: dirk.guldi@fau.de*
[b]*Área de Química Orgánica, Instituto de Bioingeniería, Universidad Miguel Hernández, Avda. de la Universidad s/n, 03203 Elche, Spain. E-mail: fdofdez@umh.es*
[c]*Computer-Chemistry-Center, Department of Chemistry and Pharmacy, Friedrich-Alexander-University Erlangen-Nuremberg, Nägelsbachstr. 25, 91052 Erlangen, Germany*

†Electronic supplementary information (ESI) available: (I) Listing of the general experimental methods; (II) description of the synthetic procedures; (III) NMR and MALDI-TOF spectra; (IV) electrochemical and spectro-electrochemical measurements; (V) figures and tables from the photophyscial characterization; (VI) details on theoretical calculations. See DOI: 10.1039/d1nr08523a

Recently, several families of molecular building blocks have been demonstrated to be SF-active: these include first and foremost linear acenes[12,44–52] such as tetracene and pentacene, followed by carotenoids,[53–59] diketopyrrolopyrroles,[26,32,60–67] and rylenes[31,68–76] such as perylene- and terrylene-diimides. Lately, we shifted our attention to a dimer of perylene-monoimide with napthylene as a spacer (**PMI-N-PMI**). At room temperature, **PMI-N-PMI** shows fast G-TTA-UC rather than SF. But, G-TTA-UC could be suppressed by either lowering the temperature (~140 K) or using polar solvents (benzonitrile).[10] Both approaches helped stabilize the correlated triplet pair $^1(T_1T_1)$. The strong electronic coupling between the two PMIs prevented, however, the disentanglement into $(T_1 + T_1)$. Instead, the electronic ground state was reinstated *via* TTA.

In this contribution, we build on our findings regarding **PMI-N-PMI** and explore two novel SF aspects. First, we changed the dipole moment in the dimers by replacing perylene-monoimides (PMI) with perylene-diimides (PDI). Second, we altered the intramolecular interactions, while restricting the rotational freedom, by changing from a napthylene- to a phenylene-spacer (Fig. 1). By doing so, we shed light on the impact of dipole moments within monomers and dimers and the intramolecular exchange coupling on the SF-mechanism, -kinetics, and -efficiencies.

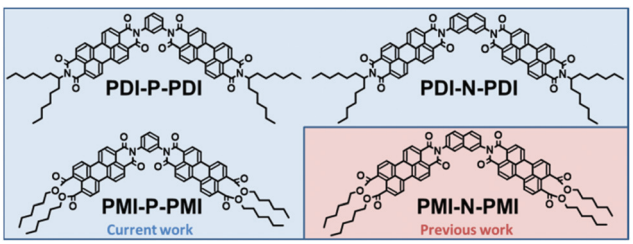

Fig. 1 Chemical structures of PDI-P-PDI, PDI-N-PDI, PMI-P-PMI, and PMI-N-PMI.

Results and discussion

Synthesis

PDI-N-PDI, **PDI-P-PDI**, and **PMI-P-PMI** were synthesized by condensation of a perylenemonoanhydride, either PMAMI[77] (for the first two compounds) or PMADE[78] (for the latter), with the corresponding arylenediamine using molten imidazole as solvent and DMAP as catalyst (Scheme 1) in 61%, 51%, and 51% yields, respectively (see ESI† for details). It is interesting to note that **PDI-P-PDI** has been previously synthesized in 5% yield after 4 days of reaction,[79] while our method afforded it in 51% after 5 hours. Characterization was carried out by ^{1}H-NMR, ^{13}C-NMR, FT-IR, UV-vis, and HR-MALDI-TOF (Fig. S1–S6†).

Theory

We used gas-phase calculations to investigate inherent geometrical differences as follows; firstly, we focused on the geometries of the PMI and PDI base core (Fig. S54†). PDI with fused imide groups displayed a large-area coplanar conformation, whereas in **PMI-Ref** the perylene core exhibits torsion of approximately 5° due to the break of coplanarity caused by the terminal ester groups. Optimized distances of non-covalent interactions between oxygen (O) and hydrogen (H) atoms in the bay region and details on the coplanarity were also analyzed (Table S9†). Overall, **PMI-P-PMI** and **PMI-N-PMI** exhibited lower electron-deficiency in the monomeric planes, when compared to **PDI-P-PDI** and **PDI-N-PDI**. Their lower degree of

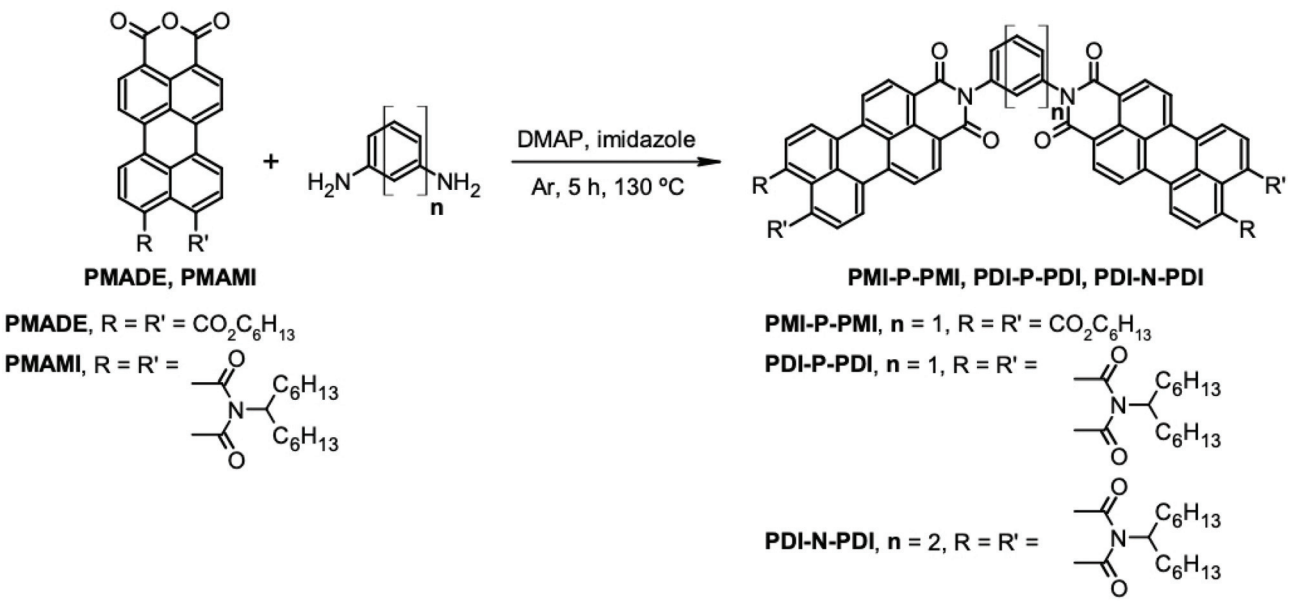

Scheme 1 Synthesis of the phenylene- and naphthylene-linked perylene-monoimide and perylene-diimides dimers PMI-P-PMI, PDI-P-PDI, and PDI-N-PDI.

coplanarity is responsible (Table S9, Fig. S55†). In-depth analyses were carried out among the central spacers. Longer distances between neighboring O- and H-atoms in the bay regions, 3.5 Å for **PDI-N-PDI** and 3.2 Å for **PMI-N-PMI** *versus* 3.0 Å for **PDI-P-PDI** and **PMI-P-PMI**, are consistent with larger twist-angles between monomer- and spacer-planes, approximately 89.5° for **PDI-N-PDI** and 77° for **PMI-P-PMI** *versus* 69° for **PDI-P-PDI** and **PMI-P-PMI**. At this point, we conclude a less-hindered rotation for the napthylene-spaced dimers (Table S9†).

Next, we examined the molecular electrostatic potentials (MEP). We found that the negative surfaces around the O-atoms overlap well with the positive ones associated with the H-atoms of the spacer, perhaps indicating C–H···O hydrogen bonds, which also result in larger dipole moments in the phenylene-spaced dimers (Table S10†).[80–83] The resulting geometry leads to highest occupied molecular orbitals (HOMOs) and lowest unoccupied molecular orbitals (LUMOs) of, for example, **PMI-P-PMI** that are delocalized over the two PMIs without any appreciable coefficients on the spacer itself (Table S11†). The situation is different for the napthylene spacers. HOMOs are delocalized across the entire molecule including the spacers themselves. Only the LUMOs lack contributions on the spacers (Table S12†). Finally, HOMO and LUMO of **PDI-P-PDI** are distinctly localized on one or the other of the two PDIs. A more heterogeneous charge distribution is the consequence (Table S13†).

Photophysics

Monoimides *versus* diimides. First we focused on the comparison between the previously reported **PMI-N-PMI**[10] and the newly synthesized **PDI-N-PDI**. The steady-state absorption spectra reveal a 20 nm bathochromic shift and a doubling of the extinction coefficients for **PDI-N-PDI** relative to **PMI-N-PMI** for all solvents (toluene – Tol, tetrahydrofuran – THF, benzonitrile – BN) and did not reveal any signs of aggregation (Fig. 2). The extinction coefficients of **PDI-N-PDI** were independently confirmed by a comparison with **PDI-Ref**,[84] a bay-substituted PDI monomer as reference (Fig. S7†). The bay-substitution prevented the monomer from forming aggregates and, thus, serves as a better reference for non-aggregating dimer. The extinction coefficients in **PDI-N-PDI** are nearly three times higher than **PDI-Ref** (Fig. S13†).

Steady-state fluorescence measurements of **PDI-N-PDI** revealed similar fluorescence quantum yields (FQY) to **PMI-N-PMI**. The lowest FQYs were found in THF, with higher values in Tol and BN (Fig. 2). For **PDI-N-PDI**, the FQYs are 89% in Tol, 38% in THF, and 69% in BN. Compared to **PDI-Ref** with 100% in Tol, 96% in THF, and 85% in BN, the fluorescence is quenched in **PDI-N-PDI** (Fig. S13, Table S1†).

Regarding the excitation spectra, similar changes in the oscillator strength upon probing different solvents, as in the case of **PDI-N-PDI**, were interpreted as CT contributions to (S_1).[47] Regarding the fluorescence spectra, significant changes contrast the case of **PDI-N-PDI** and confirm the involvement of CT. A closer look into this matter came from recording time-resolved emission spectra (TRES) for **PDI-N-PDI** (Fig. S19b†). PDI-centered fluorescence maxima evolve for **PDI-N-PDI** in BN at 537 and 575 nm. As time progresses, the former splits into 554 and 578 nm maxima, while the latter remains largely unchanged (Fig. S19b†). We ascribe these observations to an equilibrium between a fluorescent $(S_1S_0)/(S_1S_0)_{Sol}$ and an emissive $(S_1S_0)_{CS}$ – *vide infra*.

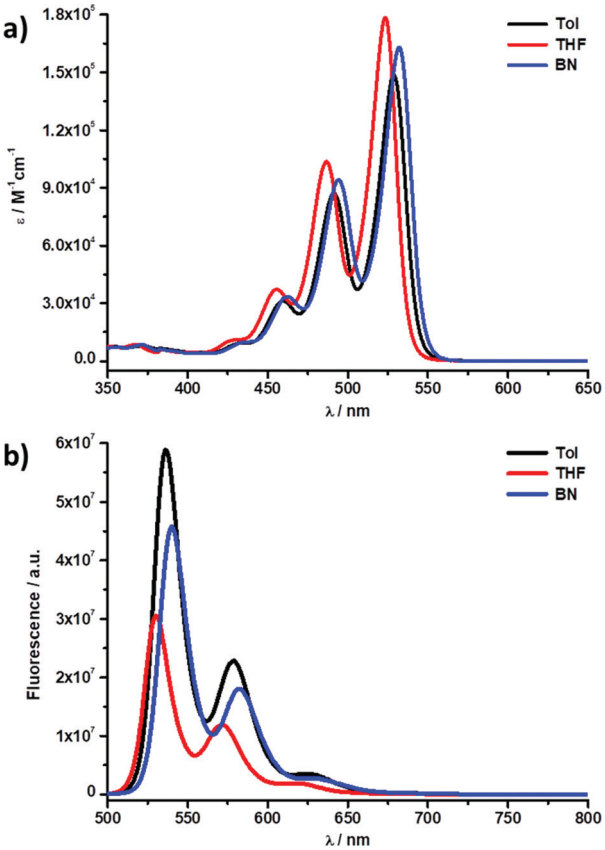

Fig. 2 Absorption (a) and fluorescence (b) spectra of **PDI-N-PDI** in Tol (black), THF (red), and BN (blue), respectively.

In time-correlated single-photon counting (TCSPC) measurements, a mono-exponentially decaying fluorescence with a 3.6 ns lifetime was found for **PDI-N-PDI** in Tol. The fluorescent decay of **PDI-N-PDI** is doubly exponential in THF and BN. The lifetimes are 1.4 and 3.7 ns in THF and 2.5 and 26.0 ns in BN (Fig. S19, Table S3†). Only a single fluorescent species was found for **PMI-N-PMI**,[10] regardless of the solvent. In other words, multiple, solvent dependent, fluorescent species are only present in **PDI-N-PDI**. It is notable that **PDI-Ref** featured only a mono-exponential fluorescence decay in all solvents (Fig. S17, Table S3†).

Next, we performed electrochemical and spectro-electrochemical (SEC) measurements to determine the reduction and oxidation potentials of **PMI-P-PMI**, **PDI-P-PDI**, **PMI-N-PMI**, and **PDI-N-PDI** and also to identify the spectral fingerprints of their one-electron reduced and oxidized forms. One-electron reduction and oxidation for **PDI-N-PDI** occurred at −0.84 and +1.48 V *versus* Fc/Fc^+, respectively (Fig. S8†).

In SEC assays with **PDI-N-PDI**, applying a negative potential led to the fully reversible formation of the one-electron reduced form, which features maxima at 700 and 960 nm. In contrast, a positive potential resulted in the irreversible formation of the one-electron oxidized form. Here, a rather broad maximum at about 600 nm evolved (Fig. 3). Both the one-electron reduced and oxidized SEC fingerprints agree fairly well with previous reports.

Finally, time-resolved transient absorption measurements, on the femto- (fs-TAS, 0 ps – 5.5 ns) and nanosecond (ns-TAS, 0 ns – 350 μs) timescales, revealed details about the excited-state kinetics and SF-process of **PDI-N-PDI** and its differences to **PMI-N-PMI**. TAS data were evaluated *via* GloTarAn[85] target analyses. First, we refocus on **PMI-N-PMI**.[10] Our previous study revealed that **PMI-N-PMI** is subject to an efficient up-conversion *via* geminate triplet–triplet recombination (G-TTA-UC). At room temperature, G-TTA-UC inhibits the observation of any triplet excited state.

Independent confirmation for TTA-UC came from steady-state and time-resolved fluorescence measurements. Lowering the temperature, on the one hand, and/or turning to polar solvents, on the other, assisted in deactivating the up-conversion and activating SF. Next to up-conversion *via* G-TTA-UC, a mediating $(S_1S_0)_{CT}$, which is based on a rather strong mixing between charge transfer, singlet, and triplet excited states, is involved.[10]

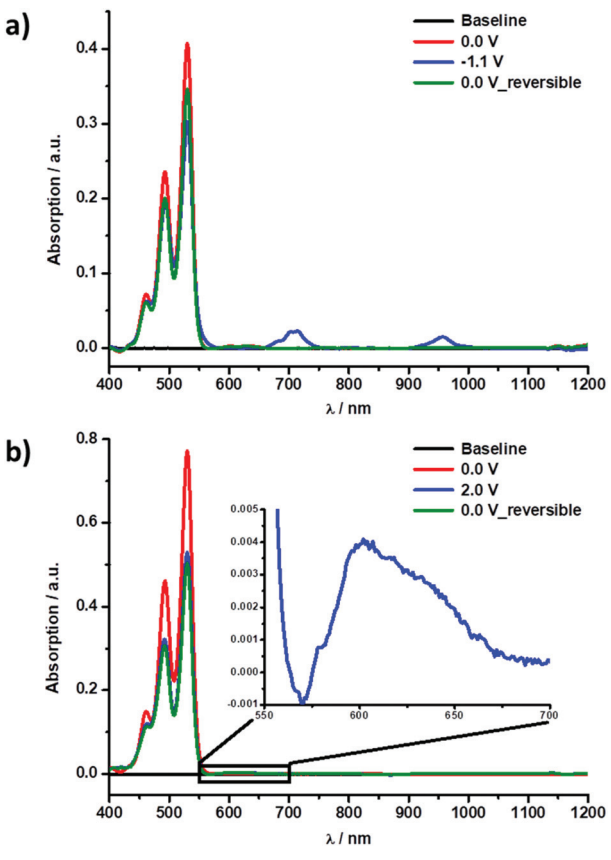

Fig. 3 Spectro-electrochemical features of the (a) one-electron reduced and (b) one-electron oxidized species of **PDI-N-PDI** in a toluene/acetonitrile solution (4/1 v/v) with 0.1 M tetrabutylammonium hexafluorophosphate ($TBAPF_6$) as supporting electrolyte.

Turning to **PDI-Ref**, photoexcitation (λ_{ex} = 480 nm, 400 nJ) led to formation of broad maxima at 680 and 910 nm, together with minima at 463, 533, 581, and 625 nm. The former two minima represent ground-state bleaching (GSB), while the latter two stem from stimulated emission (SE).

On the fs-TAS timescale, all features red-shift within picoseconds regardless of the solvent (Tol, THF, BN). The corresponding transition relates to solvent reorganization of the initially formed (S_1) and results within roughly 7 ps in $(S_1)_{Sol}$. Subsequently, the ground state is reinstated within about 5 ns in all solvents. Measurements on the ns-TAS timescale corroborate the $(S_1)_{Sol}$ deactivation and that no triplet excited state *via*, for example, intersystem crossing (ISC), is formed (Fig. S24–S29, Table S4†).

Switching to **PDI-N-PDI**, photoexcitation (λ_{ex} = 480 nm, 400 nJ) led to the instantaneous formation of broad maxima at 705 and 920 nm, together with GSB and SE minima at 455, 527, 571, and 620 nm, respectively. These are the characteristics of (S_1S_0). On the fs-TAS timescale, a red-shift of GSB, SE, and maxima indicates solvent reorganization in all solvents (Tol, THF, BN). This solvent reorganization takes about 1 ps and transforms (S_1S_0) into $(S_1S_0)_{Sol}$. In Tol, $(S_1S_0)_{Sol}$ experiences direct ground-state recovery, which is completed after 3.50 ns without the population of any other intermediates (Fig. S30†). In stark contrast, in THF and BN the $(S_1S_0)_{Sol}$ features are replaced by a new species after 1.40 and 1.68 ns, respectively. The newly evolving maximum at 955 nm is most notable. The fs-TAS timescale is, however, insufficient to resolve all the characteristics of this species fully, making it necessary to examine it more closely with ns-TAS. Here, the full range of the new species could be resolved. It included maxima at approximately 600, 700, and 955 nm. All of them are in perfect agreement with the spectral fingerprints of the radical anion and radical cation features seen in the SEC assays (Fig. 3), which was illustrated by an overlay of the individual species (Fig. 5a). From this agreement, we conclude that a symmetry-breaking charge separated $(S_1S_0)_{CS}$ state evolves. It is notable that in BN, the spectral fingerprints are somewhat sharper than in THF, which points to some solvent stabilization of $(S_1S_0)_{CS}$ (Fig. 4 and S34†). This stabilization was furthermore corroborated by means of TRES in BN – *vide supra*. The stabilization governs the subsequent $(S_1S_0)_{CS}$ decay. For example, $(S_1S_0)_{CS}$ continues in THF to transition after 7.62 ns into two subsequent species. They both exhibit maxima at 440, 500, and 555 nm next to GSB at 427 nm rather than any NIR transient or SE (Fig. 4).

All of these features reflect the triplet excited state. Triplet–triplet sensitization measurements (Fig. S23†) with a *N*-methylfulleropyrrolidine (*N*-MFP) sensitizer (Fig. S20†) and an overlay of the respective species confirmed our spectral assignment (Fig. 5b). We therefore come to the conclusion that these species relate to the correlated $^1(T_1T_1)$ and uncorrelated triplet pair (T_1 + T_1) states. Their lifetimes are 35.3 ns and 81.7 μs, respectively. In other words, $(S_1S_0)_{CS}$ mediates in

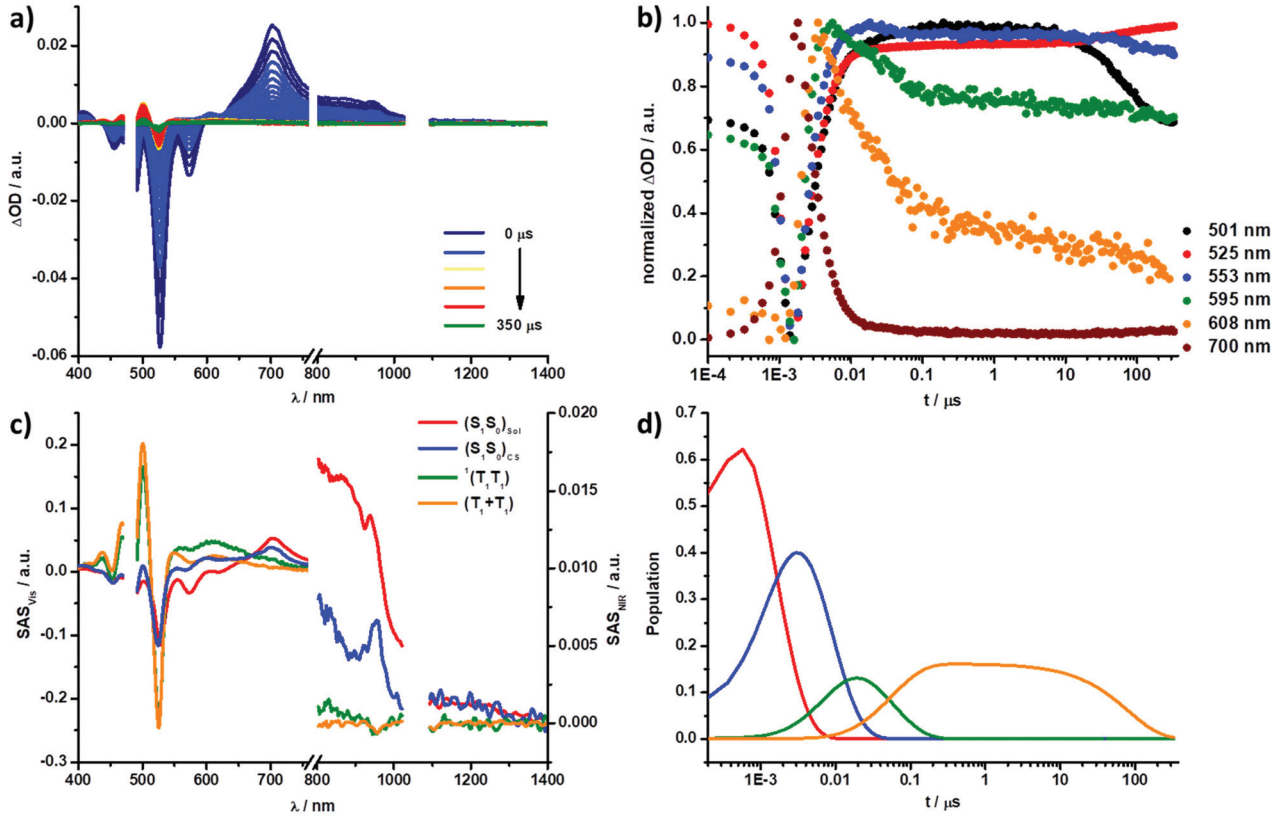

Fig. 4 (a) Ns-TAS spectra (λ_{ex} = 480 nm, 400 nJ) of **PDI-N-PDI** in THF with time delays between 0–350 µs. (b) Respective time absorption profiles at 501, 525, 553, 595, 608, and 700 nm. (c) Deconvoluted and GSB normalized ns-TAS spectra of the solvent relaxed singlet excited state (S_1S_0) (red), charge separated state $(S_1S_0)_{CS}$ (blue), singlet correlated triplet pair $^1(T_1T_1)$, and uncorrelated triplet pair (T_1 + T_1) of **PDI-N-PDI** in THF as obtained by target analysis. (d) Respective population kinetics.

THF the population of the triplet excited states. In BN, only a single species of, however, low intensity and a long lifetime of 161.6 µs was found. From a spectroscopic comparison, we conclude that it is the triplet excited state (Fig. S34†). As above-mentioned, solvent stabilization of $(S_1S_0)_{CS}$ goes hand-in-hand with a longer lifetime of 31.44 ns, but seems to prevent population of $^1(T_1T_1)$. Instead, only (T_1) is formed either as a product of charge recombination or as a product of a slow and inefficient ISC (Table S5†).

The triplet quantum yield (TQY) was determined by normalizing the GSB in the deconvoluted species-associated spectra (SAS) derived in the GloTarAn target analyses (see ESI† for details), resulting in a TQY for **PDI-N-PDI** in THF of 36%.‡

An alternative mechanism for the population of the different triplet excited states implies charge recombination from the charge separated state and, in turn, population of two isolated triplets, rather than a correlated triplet pair.[86] The long-lived triplet excited states might stem from conformational changes that occur on longer time scales.[86] In the past, such a behaviour has been reported for pentacene dimers, for which rather long distances between pentacenes assisted in decoupling them and in supporting the described SF mechanism.[86] Under such conditions, rotational freedom of the naphtylene-linker is likely to be responsible for decoupling the perylene-diimides. Considering the complete absence of a nanosecond-lived triplet feature in BN renders a CS-mediated mechanism more reasonable.

At this point, we conclude that when utilizing perylene-monoimides, a CT pathway enables SF. It takes, however, low temperatures and/or polar environments to suppress up-conversion *via* G-TTR-UC and to detect SF. Instead, when using perylene-diimides, a CS pathway is activated. It, however, mediates SF and, in turn, $^1(T_1T_1)$ population, only in moderately polar environments such as THF. In a very polar environment such as BN, $(S_1S_0)_{CS}$ is a trap state, which shuts down any SF.[87] In this scenario, only one (T_1) species is formed as a product of charge recombination.§

‡It should be mentioned that the overlap of GSB and triplet excited state features hampers a precise determination of its TQY to its full extent. Furthermore the yield for the transition from $^1(T_1T_1)$ to (T_1 + T_1) is around 90%.

§Here it should be noted that the photo-salient feature of the naphthylene-linker could also, in theory, lead to the population of PDI excited states *via* energy transfer, especially with excitations less than 387 nm.

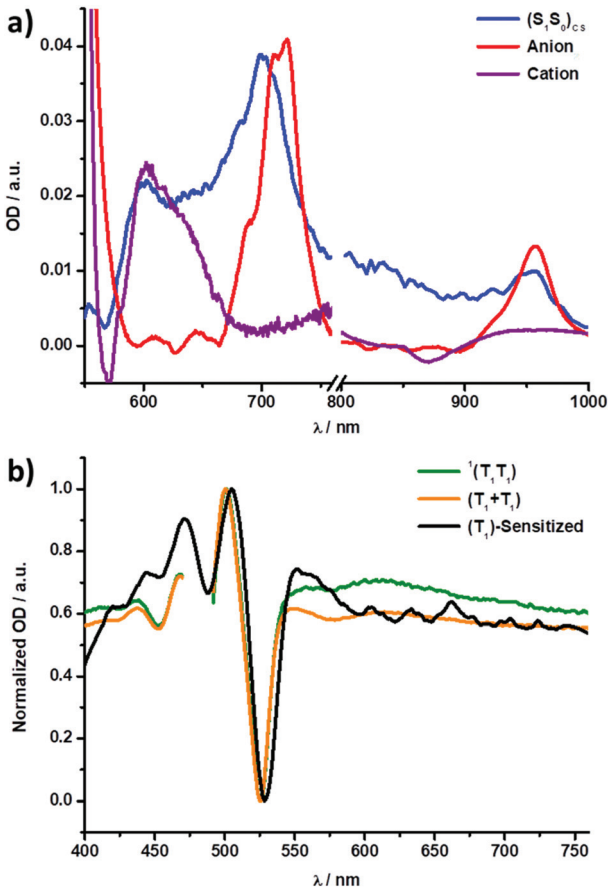

Fig. 5 Spectral overlay of (a) the one-electron reduced species (red), the one-electron oxidized species (purple) from SEC of **PDI-N-PDI** in toluene/acetonitrile solution (4/1 v/v), and $(S_1S_0)_{CS}$ (blue) from ns-TAS of **PDI-N-PDI** in toluene/acetonitrile solution (4/1 v/v), after adjusting the intensities of the spectra and (b) the sensitized (T_1) (black), $^1(T_1T_1)$ (green), and (T_1 + T_1) (orange) from nsTA of **PDI-N-PDI** in THF.

Phenylene- ***versus*** **naphthylene-linker.** The same set of experiments was conducted for the phenylene-spaced PMI and PDI dimers: **PMI-P-PMI** and **PDI-P-PDI** to shed light onto emerging differences between phenylene- and napthylene-spacers. Overall, the results of the steady-state absorption and fluorescence measurements with **PMI-P-PMI** and **PDI-P-PDI** were exactly the same as summarized for **PMI-N-PMI** and **PDI-N-PDI**. Notably, the extinction coefficients were lower than those of the naphthylene-spaced dimers, but higher than those of the references (Fig. S12 and S14, Table S1†).

The FQYs are Tol > BN > THF. Despite the fact that the FQYs of **PMI-P-PMI** and **PDI-P-PDI** were the lowest in THF, they were still rather high when compared to **PMI-N-PMI** and **PDI-N-PDI** with values of 68% and 73%, respectively (Fig. S12 and S14, Table S1†). This *per se* indicates the worse performance of phenylene spacers to drive SF in PMIs and PDIs. Deeper insights came from the TCSPC measurements. For **PDI-P-PDI**, the fluorescence of only one species was found in Tol, while two fluorescent species were detected in THF and BN. **PMI-P-PMI** featured much like the observations for **PMI-N-PMI** a mono-exponential fluorescence decay in all solvents. Also, their respective lifetimes are quite similar with roughly 4 ns for **PMI-P-PMI** and **PMI-N-PMI** (Fig. S16, Table S2†). What changed, however, was the lifetime of longer-lived species, which was for **PDI-P-PDI** in THF much longer than for **PDI-N-PDI** (Fig. S18, Table S3†).

SEC measurements were successful in terms of reducing **PMI-P-PMI** with its 650 nm fingerprint, but its oxidation failed (Fig. S9†). For **PDI-P-PDI**, both reduction and oxidation resulted in characteristic fingerprints at 700/960 and 600 nm, respectively (Fig. S10†). Overall, the SEC fingerprints are nearly identical for **PMI-P-PMI**/**PDI-P-PDI** and **PMI-N-PMI**/**PDI-N-PDI**.

Turning to fs-TAS and ns-TAS measurements, we first focused on **PMI-P-PMI**. Measurements were conducted at room and cryogenic (140 K) temperatures, to corroborate the temperature dependent triplet–triplet interactions as seen in **PMI-N-PMI**. At room temperature, the deactivation sequences of **PMI-P-PMI** and **PMI-N-PMI** are identical. First, population of the singlet excited state (S_1S_0) takes place. Second, (S_1S_0) transitions to a state with charge-transfer character $(S_1S_0)_{CT}$. Finally, $(S_1S_0)_{CT}$ populates a species, which has the same spectral shape as (S_1S_0) before the ground state is recovered, indicating up-conversion *via* G-TTR into $(S_1S_0)_{UC}$ (Fig. S35–S37, Table S6†). Unlike **PMI-N-PMI**, a change in solvent polarity did not influence the deactivation sequence of **PMI-P-PMI.**¶

Fs-TAS and ns-TAS measurements at 140 K revealed the population of the correlated triplet pair state $^1(T_1T_1)$, mixed with a significant CT character, noticeable by a shoulder at around 650 nm especially in BN and at 140 K. This is very much like **PMI-N-PMI**, albeit with much lower efficiency (Fig. S38, Table S6†).‖ The triplet excited state features, that is, a maximum at 530 nm and a GSB at 510 nm, were furthermore confirmed through triplet–triplet sensitization measurements, using anthracene (Fig. S20†) as sensitizer (Fig. S21†). Overall the same SF-mechanism is applicable to **PMI-N-PMI** and **PMI-P-PMI** (Fig. S39–S47, Table S7†). But, the overall SF-efficiency, namely the TQY of $^1(T_1T_1)_{CT}$, is with 4.1% very moderate and, as such, lower than in **PMI-N-PMI.****

Switching to **PDI-P-PDI**, its deactivation pattern was quite similar to **PDI-N-PDI**, with, however, one notable difference. In Tol, photoexcitation generates (S_1S_0), which undergoes solvent relaxation to afford $(S_1S_0)_{Sol}$ and ground state recovery. In THF and BN, $(S_1S_0)_{Sol}$ converts into $(S_1S_0)_{CS}$ with 22.56 and 41.64 ns, respectively (Fig. S48–S53†). Spectroscopic evidence came in the form of the characteristic 600, 700, and 955 nm fingerprints. But, unlike **PDI-N-PDI**, neither the correlated $^1(T_1T_1)$ nor the uncorrelated triplet pair (T_1 + T_1) state evolved. Instead, in both THF and BN only one long-lived state is

¶Steady state and TCSPC measurements at 140 K led to a red-shifting and narrowing of the absorption and fluorescence features next to a decreasing of the lifetimes (Fig. S15 and S16, Table S2†).

‖For **PMI-N-PMI**, polar solvents facilitated and allowed the population of correlated triplet pairs.

**Obtained *via* normalizing the GSB in the obtained species associated spectra (SAS) from GloTarAn target analysis – see ESI† for more details.

formed as a product of charge-recombination (Table S8†), which we correlate to a single triplet excited state $^3(S_0T_1)$ due to its similar appearance and lifetime to the sensitized (T_1) (Fig. S22†).

The consequence of replacing a naphthylene-spacer with a phenylene-spacer is that the SF-efficiency is either reduced, in the case of **PMI-P-PMI**, or even shut down, in the case of **PDI-P-PDI**. These changes occur despite the closer inter-PMI and -PDI distances in **PMI-P-PMI** and **PDI-P-PDI**. A likely rationale is based on the geometrical restrictions of the free rotations. Weaker electronic couplings and interactions between the two PMIs and PDIs are due to the phenylene-spacers. Theory presented another key difference between the phenylene- and naphthylene-spacers. We probed the hole (h^+) and electron (e^-) distributions, on one hand, and the excitation assignments of the $S_0 \rightarrow S_1$ transition, on the other hand (Table S13†).[88,89] Both h^+ and e^- distributions in **PMI-P-PMI** and **PDI-P-PDI** are almost identical. They are localized on both PMIs/PDIs, but not on the phenylene-spacers. This sheds light onto the (S_1) nature in **PMI-P-PMI** and **PDI-P-PDI**, namely locally excited states, and explains the poor SF-efficiency. For **PMI-N-PMI** and **PDI-N-PMI**, e^- distributions are on the naphthylene-spacers, while h^+ distributions are on both PMIs/PDIs. This explains the generally better SF-performance in the naphthylene-spaced dimers. In terms of excitation assignments, **PMI-P-PMI** showed evenly degenerate and delocalized transitions, whereas **PDI-P-PDI** showed evenly degenerate but localized transitions. Taking a closer look at **PMI-N-PMI**, it featured a transition with 56.6% partial CT character, whereas the transition in **PDI-N-PDI** is composed of 61.6% partial and 8.7% full CT character (Table S13†).

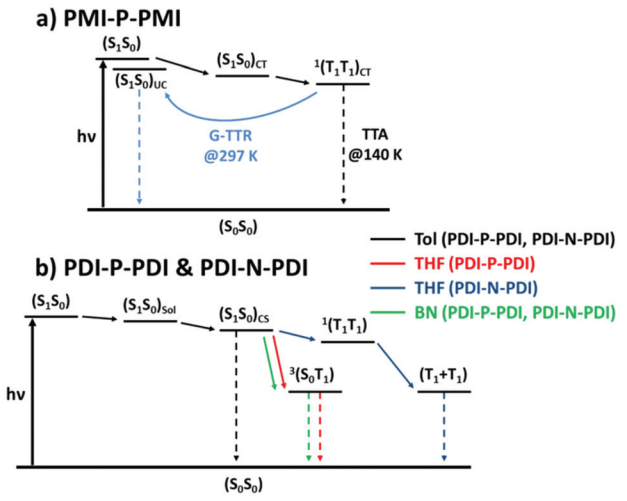

Fig. 6 General mechanistic schemes illustrating the deactivation mechanism of **PMI-P-PMI** (a) with all observed transitions at room temperature and 140 K together with the respective deactivation mechanisms of **PDI-P-PDI** and **PDI-N-PDI** (b) contingent on the utilized solvent.

Conclusions

Building upon on our previous study of a naphthylene-spaced perylene-monoimide dimer (**PMI-N-PMI**) we exchanged, on the one hand, the chromophore from a perylene-monoimide to a perylene-diimide and, on the other, the spacer from a naphthylene to a phenylene and investigated the effects on SF. In **PMI-N-PMI**, SF is mediated *via* a CT state but needs to overcome G-TTR-UC, by either lowering the temperature or using a polar solvent. In **PDI-N-PDI**, SF is mediated *via* a CS state, in which solvent polarity plays a crucial role as it either enables, in THF, or suppresses, in BN, the population of $^1(T_1T_1)$. The change in mechanism between perylene-monoimides and perylene-diimides relates to the differences in MEP surface area and deviations from coplanarity. Immediate consequences are changes in dipole moment and geometry vector.

Changing the spacer from naphthylene to phenylene exerts no notable effects on the SF. The only notable difference is the lower efficiency in **PMI-P-PMI** and **PDI-P-PDI** relative to **PMI-N-PMI** and **PDI-N-PDI**. The closer proximity in the phenylene-spacers comes at the expense of a higher polarization magnitude and no communication across the spacer as seen in **PDI-P-PDI**, where SF is absent. For the naphthylene-spacer we observe overall stronger interactions like in **PDI-N-PDI**. The spacer is part of the excited state polarization and together with a lower MEP results in the right communication between the PDIs/PMIs. This minimizes loss channels and, in turn, increases the population of $^1(T_1T_1)$. Fig. 6 illustrates the deactivation mechanisms in **PMI-N-PMI**, **PDI-N-PDI**, **PMI-P-PMI**, and **PDI-P-PDI** as a function of temperature and solvent polarity.

Author contributions

I. P. and P. M. G. performed the photophysical measurements. D. G.-M. performed the synthesis. Y. B., R. C. and T. C. performed the theoretical calculations. The manuscript was written through contributions of all authors. All authors have given approval to the final version of the manuscript.

Conflicts of interest

There are no conflicts to declare.

Acknowledgements

This work was supported by the European Regional Development Fund "A way to make Europe", the Spanish Ministerio de Ciencia e Innovación/Agencia Estatal de Investigación (PID2019 109200GB-I00) and the "Solar Energy goes Hybrid" Initiative of the Bavarian Ministry for Science, Culture and Education (SolTech). Y. B. acknowledges a fellowship from the Chinese Scholarship Council.

Notes and references

1 W. Shockley and H. J. Queisser, *J. Appl. Phys.*, 1961, **32**, 510–519.
2 S. Rühle, *Sol. Energy*, 2016, **130**, 139–147.
3 J. Xia, S. N. Sanders, W. Cheng, J. Z. Low, J. Liu, L. M. Campos and T. Sun, *Adv. Mater.*, 2017, **29**, 1601652.
4 A. Rao and R. H. Friend, *Nat. Rev. Mater.*, 2017, **2**, 17063.
5 B. Ehrler, M. W. B. Wilson, A. Rao, R. H. Friend and N. C. Greenham, *Nano Lett.*, 2012, **12**, 1053–1057.
6 J. Michl, *Mol. Front. J.*, 2019, **03**, 1–8.
7 M. K. Gish, N. A. Pace, G. Rumbles and J. C. Johnson, *J. Phys. Chem. C*, 2019, **123**, 3923–3934.
8 M. B. Smith and J. Michl, *Chem. Rev.*, 2010, **110**, 6891–6936.
9 M. B. Smith and J. Michl, *Annu. Rev. Phys. Chem.*, 2013, **64**, 361–386.
10 I. Papadopoulos, D. Gutiérrez-Moreno, P. M. McCosker, R. Casillas, P. A. Keller, Á. Sastre-Santos, T. Clark, F. Fernández-Lázaro and D. M. Guldi, *J. Phys. Chem. A*, 2020, **124**, 5727–5736.
11 T. Ullrich, D. Munz and D. M. Guldi, *Chem. Soc. Rev.*, 2021, **50**, 3485–3518.
12 B. J. Walker, A. J. Musser, D. Beljonne and R. H. Friend, *Nat. Chem.*, 2013, **5**, 1019–1024.
13 N. Monahan and X.-Y. Zhu, *Annu. Rev. Phys. Chem.*, 2015, **66**, 601–618.
14 K. M. Felter and F. C. Grozema, *J. Phys. Chem. Lett.*, 2019, **10**, 7208–7214.
15 R. Casillas, M. Adam, P. B. Coto, A. R. Waterloo, J. Zirzlmeier, S. R. Reddy, F. Hampel, R. McDonald, R. R. Tykwinski, M. Thoss and D. M. Guldi, *Adv. Energy Mater.*, 2019, **9**, 1802221.
16 M. J. Y. Tayebjee, K. N. Schwarz, R. W. MacQueen, M. Dvořák, A. W. C. Lam, K. P. Ghiggino, D. R. McCamey, T. W. Schmidt and G. Conibeer, *J. Phys. Chem. C*, 2016, **120**, 157–165.
17 A. N. Stuart, P. C. Tapping, E. Schrefl, D. M. Huang and T. W. Kee, *J. Phys. Chem. C*, 2019, **123**, 5813–5825.
18 C. Gao, S. K. K. Prasad, B. Zhang, M. Dvořák, M. J. Y. Tayebjee, D. R. McCamey, T. W. Schmidt, T. A. Smith and W. W. H. Wong, *J. Phys. Chem. C*, 2019, **123**, 20181–20187.
19 L. Wang, Y. Olivier, O. V. Prezhdo and D. Beljonne, *J. Phys. Chem. Lett.*, 2014, **5**, 3345–3353.
20 N. V. Korovina, N. F. Pompetti and J. C. Johnson, *J. Chem. Phys.*, 2020, **152**, 040904.
21 R. Casillas, I. Papadopoulos, T. Ullrich, D. Thiel, A. Kunzmann and D. M. Guldi, *Energy Environ. Sci.*, 2020, **13**, 2741–2804.
22 T. Zeng, P. Goel and M. Nooijen, *J. Phys. Chem. Lett.*, 2016, **7**, 1351–1358.
23 E. Busby, J. Xia, Q. Wu, J. Z. Low, R. Song, J. R. Miller, X. Y. Zhu, L. M. Campos and M. Y. Sfeir, *Nat. Mater.*, 2015, **14**, 426–433.
24 J. Hu, K. Xu, L. Shen, Q. Wu, G. He, J.-Y. Y. Wang, J. Pei, J. Xia, M. Y. Sfeir, J. Hu, J. Pei, L. Shen, J. Xia, M. Y. Sfeir, J.-Y. Y. Wang, K. Xu and Q. Wu, *Nat. Commun.*, 2018, **9**, 2999.
25 S. Ito, T. Nagami and M. Nakano, *J. Phys. Chem. A*, 2016, **120**, 6236–6241.
26 C. E. Miller, M. R. Wasielewski and G. C. Schatz, *J. Phys. Chem. C*, 2017, **121**, 10345–10350.
27 S. R. Reddy, P. B. Coto and M. Thoss, *J. Phys. Chem. Lett.*, 2018, **9**, 5979–5986.
28 P. M. Zimmerman, F. Bell, D. Casanova and M. Head-Gordon, *J. Am. Chem. Soc.*, 2011, **133**, 19944–19952.
29 E. G. Fuemmeler, S. N. Sanders, A. B. Pun, E. Kumarasamy, T. Zeng, K. Miyata, M. L. Steigerwald, X. Y. Zhu, M. Y. Sfeir, L. M. Campos and N. Ananth, *ACS Cent. Sci.*, 2016, **2**, 316–324.
30 W. L. Chan, T. C. Berkelbach, M. R. Provorse, N. R. Monahan, J. R. Tritsch, M. S. Hybertsen, D. R. Reichman, J. Gao and X. Y. Zhu, *Acc. Chem. Res.*, 2013, **46**, 1321–1329.
31 C. Schierl, A. Niazov-Elkan, L. J. W. Shimon, Y. Feldman, B. Rybtchinski and D. M. Guldi, *Nanoscale*, 2018, **10**, 20147–20154.
32 I. Papadopoulos, M. J. Álvaro-Martins, D. Molina, P. M. McCosker, P. A. Keller, T. Clark, Á. Sastre-Santos and D. M. Guldi, *Adv. Energy Mater.*, 2020, **10**, 2001496.
33 M. T. Trinh, A. Pinkard, A. B. Pun, S. N. Sanders, E. Kumarasamy, M. Y. Sfeir, L. M. Campos, X. Roy and X. Y. Zhu, *Sci. Adv.*, 2017, **3**, e1700241.
34 G. D. Scholes, *J. Phys. Chem. A*, 2015, **119**, 12699–12705.
35 G. B. Piland, J. J. Burdett, R. J. Dillon and C. J. Bardeen, *J. Phys. Chem. Lett.*, 2014, **5**, 2312–2319.
36 M. Chen, Y. J. Bae, C. M. Mauck, A. Mandal, R. M. Young and M. R. Wasielewski, *J. Am. Chem. Soc.*, 2018, **140**, 9184–9192.
37 T. S. Lee, Y. L. Lin, H. Kim, R. D. Pensack, B. P. Rand and G. D. Scholes, *J. Phys. Chem. Lett.*, 2018, **9**, 4087–4095.
38 M. J. Y. Tayebjee, S. N. Sanders, E. Kumarasamy, L. M. Campos, M. Y. Sfeir and D. R. McCamey, *Nat. Phys.*, 2017, **13**, 182–188.
39 D. Di, L. Yang, J. M. Richter, L. Meraldi, R. M. Altamimi, A. Y. Alyamani, D. Credgington, K. P. Musselman, J. L. MacManus-Driscoll and R. H. Friend, *Adv. Mater.*, 2017, **29**, 1605987.
40 T. N. Singh-Rachford and F. N. Castellano, *Coord. Chem. Rev.*, 2010, **254**, 2560–2573.
41 V. Gray, K. Moth-Poulsen, B. Albinsson and M. Abrahamsson, *Coord. Chem. Rev.*, 2018, **362**, 54–71.
42 A. B. Pun, S. N. N. Sanders, M. Y. Sfeir, L. M. Campos and D. N. Congreve, *Chem. Sci.*, 2019, **10**, 3969–3975.
43 V. Gray, A. Dreos, P. Erhart, B. Albinsson, K. Moth-Poulsen and M. Abrahamsson, *Phys. Chem. Chem. Phys.*, 2017, **19**, 10931–10939.
44 Z. Tang, S. Zhou, X. Wang, H. Liu, X. Yan, S. Liu, X. Lu and X. Li, *J. Mater. Chem. C*, 2019, 11090–11098.
45 N. V. Korovina, J. Joy, X. Feng, C. Feltenberger, A. I. Krylov, S. E. Bradforth and M. E. Thompson, *J. Am. Chem. Soc.*, 2018, **140**, 10179–10190.

46 H. Liu, R. Wang, L. Shen, Y. Xu, M. Xiao, C. Zhang and X. Li, *Org. Lett.*, 2017, **19**, 580–583.
47 A. M. Alvertis, S. Lukman, T. J. H. Hele, E. G. Fuemmeler, J. Feng, J. Wu, N. C. Greenham, A. W. Chin and A. J. Musser, *J. Am. Chem. Soc.*, 2019, **141**, 17558–17570.
48 B. S. Basel, R. M. Young, M. D. Krzyaniak, I. Papadopoulos, C. Hetzer, Y. Gao, N. T. La Porte, B. T. Phelan, T. Clark, R. R. Tykwinski, M. R. Wasielewski and D. M. Guldi, *Chem. Sci.*, 2019, **10**, 11130–11140.
49 I. Papadopoulos, J. Zirzlmeier, C. Hetzer, Y. J. Bae, M. D. Krzyaniak, M. R. Wasielewski, T. Clark, R. R. Tykwinski and D. M. Guldi, *J. Am. Chem. Soc.*, 2019, **141**, 6191–6203.
50 I. Papadopoulos, Y. Gao, C. Hetzer, R. R. Tykwinski and D. M. Guldi, *ChemPhotoChem*, 2020, **4**, 1–8.
51 S. R. Yost, J. Lee, M. W. B. Wilson, T. Wu, D. P. McMahon, R. R. Parkhurst, N. J. Thompson, D. N. Congreve, A. Rao, K. Johnson, M. Y. Sfeir, M. G. Bawendi, T. M. Swager, R. H. Friend, M. A. Baldo and T. Van Voorhis, *Nat. Chem.*, 2014, **6**, 492–497.
52 C. Hetzer, D. M. Guldi and R. R. Tykwinski, *Chem. – Eur. J.*, 2018, **24**, 8245–8257.
53 H. Rademaker, A. J. Hoff, R. Van Grondelle and L. N. M. Duysens, *Biochim. Biophys. Acta, Bioenerg.*, 1980, **592**, 240–257.
54 H. Kingma, R. van Grondelle and L. N. M. Duysens, *Biochim. Biophys. Acta, Bioenerg.*, 1985, **808**, 363–382.
55 J. Alster, T. Polívka, J. B. Arellano, P. Chábera, F. Vácha and J. Pšenčík, *Chem. Phys.*, 2010, **373**, 90–97.
56 D. M. Niedzwiedzki, D. J. K. Swainsbury, E. C. Martin, C. N. Hunter and R. E. Blankenship, *J. Phys. Chem. B*, 2017, **121**, 7571–7585.
57 C. Wang and M. J. Tauber, *J. Am. Chem. Soc.*, 2010, **132**, 13988–13991.
58 A. J. Musser, M. Maiuri, D. Brida, G. Cerullo, R. H. Friend and J. Clark, *J. Am. Chem. Soc.*, 2015, **137**, 5130–5139.
59 M. T. Trinh, Y. Zhong, Q. Chen, T. Schiros, S. Jockusch, M. Y. Sfeir, M. Steigerwald, C. Nuckolls and X. Zhu, *J. Phys. Chem. C*, 2015, **119**, 1312–1319.
60 P. E. Hartnett, E. A. Margulies, C. M. Mauck, S. A. Miller, Y. Wu, Y.-L. Wu, T. J. Marks and M. R. Wasielewski, *J. Phys. Chem. B*, 2016, **120**, 1357–1366.
61 C. M. Mauck, P. E. Hartnett, E. A. Margulies, L. Ma, C. E. Miller, G. C. Schatz, T. J. Marks and M. R. Wasielewski, *J. Am. Chem. Soc.*, 2016, **138**, 11749–11761.
62 T. Mukhopadhyay, A. J. Musser, B. Puttaraju, J. Dhar, R. H. Friend and S. Patil, *J. Phys. Chem. Lett.*, 2017, **8**, 984–991.
63 C. M. Mauck, P. E. Hartnett, Y. L. Wu, C. E. Miller, T. J. Marks and M. R. Wasielewski, *Chem. Mater.*, 2017, **29**, 6810–6817.
64 C. M. Mauck, Y. J. Bae, M. Chen, N. Powers-Riggs, Y.-L. Wu and M. R. Wasielewski, *ChemPhotoChem*, 2018, **2**, 223–233.
65 A. M. Levine, C. Schierl, B. S. Basel, M. Ahmed, B. A. Camargo, D. M. Guldi and A. B. Braunschweig, *J. Phys. Chem. C*, 2019, **123**, 1587–1595.
66 S. Masoomi-Godarzi, M. Liu, Y. Tachibana, L. Goerigk, K. P. Ghiggino, T. A. Smith and D. J. Jones, *Adv. Energy Mater.*, 2018, **8**, 1801720.
67 S. Masoomi-Godarzi, M. Liu, Y. Tachibana, V. D. Mitchell, L. Goerigk, K. P. Ghiggino, T. A. Smith and D. J. Jones, *Adv. Energy Mater.*, 2019, **9**, 1901069.
68 S. W. Eaton, L. E. Shoer, S. D. Karlen, S. M. Dyar, E. A. Margulies, B. S. Veldkamp, C. Ramanan, D. A. Hartzler, S. Savikhin, T. J. Marks and M. R. Wasielewski, *J. Am. Chem. Soc.*, 2013, **135**, 14701–14712.
69 K. Nagarajan, A. R. Mallia, V. S. Reddy and M. Hariharan, *J. Phys. Chem. C*, 2016, **120**, 8443–8450.
70 C. Mauck, K. Brown, N. Horwitz and M. R. Wasielewski, *J. Phys. Chem. A*, 2015, **119**, 5587–5596.
71 A. K. Le, J. A. Bender and S. T. Roberts, *J. Phys. Chem. Lett.*, 2016, **7**, 4922–4928.
72 Y. V. Aulin, K. M. Felter, D. D. Günbas, R. K. Dubey, W. F. Jager and F. C. Grozema, *ChemPlusChem*, 2018, **83**, 230–238.
73 A. K. Le, J. A. Bender, D. H. Arias, D. E. Cotton, J. C. Johnson and S. T. Roberts, *J. Am. Chem. Soc.*, 2018, **140**, 814–826.
74 K. M. Lefler, K. E. Brown, W. A. Salamant, S. M. Dyar, K. E. Knowles and M. R. Wasielewski, *J. Phys. Chem. A*, 2013, **117**, 10333–10345.
75 E. A. Margulies, J. L. Logsdon, C. E. Miller, L. Ma, E. Simonoff, R. M. Young, G. C. Schatz and M. R. Wasielewski, *J. Am. Chem. Soc.*, 2017, **139**, 663–671.
76 S. W. Eaton, S. A. Miller, E. A. Margulies, L. E. Shoer, R. D. Schaller and M. R. Wasielewski, *J. Phys. Chem. A*, 2015, **119**, 4151–4161.
77 H. Kaiser, J. Lindner and H. Langhals, *Chem. Ber.*, 1991, **124**, 529–535.
78 F. Ernst, T. Heek, A. Setaro, R. Haag and S. Reich, *J. Phys. Chem. C*, 2013, **117**, 1157–1162.
79 C. Lu, M. Fujitsuka, A. Sugimoto and T. Majima, *J. Phys. Chem. C*, 2016, **120**, 12734–12741.
80 R. F. W. Bader, M. T. Carroll, J. R. Cheeseman and C. Chang, *J. Am. Chem. Soc.*, 1987, **109**, 7968–7979.
81 F. Zhou, Y. Liu, Z. Wang, T. Lu, Q. Yang, Y. Liu and B. Zheng, *Phys. Chem. Chem. Phys.*, 2019, **21**, 15310–15318.
82 Z. Wang, Y. Liu, B. Zheng, F. Zhou, Y. Jiao, Y. Liu, X. Ding and T. Lu, *J. Chem. Phys.*, 2018, **148**, 194106.
83 J. S. Murray and P. Politzer, *Crystals*, 2020, **10**, 76.
84 R. Muñoz-Mármol, N. Zink-Lorre, J. M. Villalvilla, P. G. Boj, J. A. Quintana, C. Vázquez, A. Anderson, M. J. Gordon, A. Sastre-Santos, F. Fernández-Lázaro and M. A. Díaz-García, *J. Phys. Chem. C*, 2018, **122**, 24896–24906.
85 J. J. Snellenburg, S. P. Laptenok, R. Seger, K. M. Mullen and I. H. M. van Stokkum, *J. Stat. Softw.*, 2012, **49**, 1–22.
86 S. N. Sanders, E. Kumarasamy, A. B. Pun, M. T. Trinh, B. Choi, J. Xia, E. J. Taffet, J. Z. Low, J. R. Miller, X. Roy,

X.-Y. Zhu, M. L. Steigerwald, M. Y. Sfeir and L. M. Campos, *J. Am. Chem. Soc.*, 2015, **137**, 8965–8972.
87 E. A. Margulies, C. E. Miller, Y. Wu, L. Ma, G. C. Schatz, R. M. Young and M. R. Wasielewski, *Nat. Chem.*, 2016, **8**, 1120–1125.
88 X. Tang, L.-S. Cui, H.-C. Li, A. J. Gillett, F. Auras, Y.-K. Qu, C. Zhong, S. T. E. Jones, Z.-Q. Jiang, R. H. Friend and L.-S. Liao, *Nat. Mater.*, 2020, **19**, 1332–1338.
89 Z. Liu, T. Lu and Q. Chen, *Carbon*, 2020, **165**, 461–467.